


## Research

# Artificial thermal flow control on thermoelectric device by tuning electrode absorptivity

Sohei Saito<sup>1</sup> · Ayaha Yamamoto<sup>2</sup> · Yu-Jung Lu<sup>3</sup> · Takuo Tanaka<sup>4,5,6,7</sup> · Wakana Kubo<sup>1,2</sup> 

Received: 18 October 2024 / Accepted: 3 February 2025

Published online: 24 February 2025

© The Author(s) 2025 

## Abstract

Thermoelectric conversion is a direct conversion of thermal energy to electricity, triggered by the Seebeck effect. Typically, the configuration of a thermoelectric device and the absorptivity of both electrodes exhibit symmetrical optical characteristics between the hot and cold ends, and these factors usually are not expected to affect the direction of the thermal gradient. Here, we first demonstrate the ability to reverse the direction of thermal flow across a thermoelectric element by adjusting the absorptivity of electrodes at both ends in an environment with uniform thermal radiation. For example, when the metamaterial or fullerene electrodes were attached to one end a *p*-type thermoelectric element, they generated output voltages of 19.0 and -4.0 V, respectively, in an environment with uniform thermal radiation at 364 K. Using this insight, we demonstrated power generation on a  $\pi$ -shaped thermoelectric device consisting only of *p*-type thermoelectric legs by designing the absorptivity of the electrode at each end. Our findings will provide valuable insights as a device guideline for conventional thermoelectric devices.

## 1 Introduction

Thermoelectric conversion is a promising technology for converting thermal energy into electricity based on the Seebeck effect [1–8]. For example, S. Fan et al. achieved nighttime electric power generation by combining photovoltaic and thermoelectric generators [9]. Similarly, Ishii et al. have demonstrated a thermoelectric device that simultaneously harvests both radiative cooling and solar heating, highlighting the high potential of thermoelectric devices as power generation elements [10]. Conventional thermoelectric devices are typically used at an interface between the hot and cold environments where thermoelectric legs can hold a thermal gradient across them, such as between air and a human body or a nuclear battery and the outer space [11]. Consequently, conventional thermoelectric devices cannot generate electricity in environments with uniform thermal radiation, meaning that they cannot gather and recycle waste heat

Sohei Saito and Ayaha Yamamoto have equally contributed to this work.

**Supplementary Information** The online version contains supplementary material available at <https://doi.org/10.1186/s11671-025-04193-y>.

✉ Wakana Kubo, w-kubo@cc.tuat.ac.jp | <sup>1</sup>Department of Electrical and Electronics Engineering, Tokyo University of Agriculture and Technology, 2-24-16 Naka-Cho, Koganei-Shi, Tokyo 184-8588, Japan. <sup>2</sup>Department of Electrical Engineering and Computer Science, Tokyo University of Agriculture and Technology, 2-24-16 Naka-Cho, Koganei-Shi, Tokyo 184-8588, Japan. <sup>3</sup>Research Center for Applied Sciences, Academia Sinica, Taipei 11529, Taiwan. <sup>4</sup>Innovative Photon Manipulation Research Team, RIKEN Center for Advanced Photonics, Wako, Saitama 351-0198, Japan. <sup>5</sup>Metamaterials Laboratory, RIKEN Cluster for Pioneering Research, Wako, Saitama 351-0198, Japan. <sup>6</sup>Department of Physics, Faculty of Science, Gakushuin University, Tokyo 171-8588, Japan. <sup>7</sup>Institute of Post-LED Photonics, Tokushima University, Tokushima 770-8560, Japan.



diffused in our society since the environment where waste heats exist maintains thermal distributions uniform. To address this issue, we proposed a metamaterial thermoelectric conversion that creates electricity even in an environment with uniform thermal radiation by gathering thermal energy in surroundings using infrared (IR) metamaterial absorber (MA) [12]. Furthermore, we demonstrated this concept for the first time [13, 14].

The metamaterial thermoelectric device consists of a thermoelectric element loaded with the MA-fabricated Cu electrode with high absorptivity, and a control Cu electrode with negligible absorptivity in IR region. When the metamaterial thermoelectric device is put in an environment with uniform thermal radiation, the MA absorbs thermal radiation emitted from the surrounding environment and creates plasmonic local heat as absorption loss [15–18]. This plasmonic local heat is not negligible. For example, plasmonic local heat enables long-range optofluidic control [19] and has also been utilized to realize plasmonic heat transducers [20]. This plasmonic local heat conductively propagates to the thermoelectric element via a Cu electrode, creating a thermal gradient across the element, leading to thermoelectric power generation. Additionally, the metamaterial thermoelectric conversion continues to operate, meaning the metamaterial thermoelectric device will not reach thermal equilibrium. This occurs because the metamaterial thermoelectric conversion facilitates thermal exchange between the inside and outside of the furnace chamber, ensuring that the plasmonic local heat created by the MA is consistently dissipated through thermoelectric conversion [21]. These results indicate that metamaterial thermoelectric conversion enables the gathering and recycling of waste heat that could not be reused with conventional thermoelectric conversion devices. This technology has the potential to revolutionize the paradigm of energy generation by creating electricity from places that were not previously considered as energy sources.

In the driving mechanism of the metamaterial thermoelectric conversion, we concluded that the significant difference in absorptivity between the MA electrode and the control electrode at the opposite end determines the direction of thermal gradient across the thermoelectric element. Furthermore, we expect that such thermal flow occurs only when the significant difference in absorptivity between both ends is created. Here, we questioned how differences in the absorptivity of electrodes at both ends would affect the thermal flow direction. To address this issue, we explore how variations in the absorptivity of electrodes at both ends of a thermoelectric element can influence the direction of thermal flow. To our knowledge, such an investigation has not been conducted before. However, this insight also relates to the design strategy of conventional thermoelectric devices, and clarifying this is extremely important.

In this study, we examined effect of the absorptivity difference between electrodes at the ends of a thermoelectric device on the thermal flow direction across the thermoelectric element. This is because previous investigations only focused on the thermoelectric properties when the absorptivity of the electrodes at both ends of the thermoelectric element was dramatically changed. Consequently, we first demonstrate the ability to reverse the direction of thermal flow across a thermoelectric element by adjusting the absorptivity of electrodes at both ends in an environment with uniform thermal radiation. We prepared several electrodes with different absorptivity, the MA, control, and fullerene electrodes, and examined the thermoelectric performance of devices with those electrodes. Consequently, we found that even a slight difference in absorptivity between the electrodes at both ends greatly affect the direction of thermal flow across a thermoelectric element. Applying this technique to a  $\pi$ -shaped thermoelectric device consisting only of *p*-type thermoelectric legs, we demonstrated power generation on the device despite it consisting solely of *p*-type thermoelectric legs. This highlights the effectiveness of artificial thermal flow control across the thermoelectric elements. This artificial designing of the electrodes of a thermoelectric device has never been considered since most conventional thermoelectric devices are supposed to have an isotropic configuration in terms of geometry and optical absorptivity. However, the abovementioned results indicate that the absorptivity difference between both ends of a thermoelectric device cannot be ignored, influencing the direction of thermal flow across a thermoelectric element. If this trend becomes more evident through experiments, the insights gained could potentially serve as device guidelines for the design of thermoelectric conversion devices.

## 2 Experimental section

The MA consisting of Ag disk, Ag and calcium fluoride (CaF<sub>2</sub>) layers was formed on a Cu electrode with a size of 4 mm × 6 mm. The film thicknesses of Ag disk, Ag film and CaF<sub>2</sub> layer are 100, 150, and 60 nm, respectively. The periodicity and diameter of the Ag disk were 3 μm and 1.75 μm, respectively. This configuration is known as a metamaterial perfect absorber [22–24]. The fabricated area of the MA is 2.1 mm × 2.1 mm located at the center of a Cu electrode. The MA was fabricated by electron beam lithography (JEOL Ltd., JBX-6300FS) and thermal deposition (Sanyu Electron Corporation,

SVC-7TS 80) (Fig. 1a, right-side electrode) (Refer to Supplementary text S1 for details). Figure 1b presents the top-view scanning electron microscope (SEM) images of the MA array (Hitachi High-Technologies Corporation, SU8010).

The fullerene electrode was prepared by thermal deposition of fullerene powder (Aldrich, purity  $\geq 97.5\%$ ) on a polished and cleaned Cu electrode. The fullerene coating covered the entire Cu electrode, which has a larger area than that of the MA. Film thicknesses of the fullerene were varied between 100 and 400 nm (Fig. 1a, right electrode), and were measured using SEM.

The control electrode consists of Ag and  $\text{CaF}_2$  layers of 150 and 60 nm, respectively, and does not have an Ag disk on the top of the layer, leading to significantly lower absorption characteristics as shown in the black line in Fig. 1e (left-side electrode in Fig. 1a, c, d, and right-side electrode in Fig. 1d).

These electrodes were attached on a thermoelectric element by soldering paste. A *p*-type bismuth antimony telluride ( $\text{Bi}_{0.3}\text{Sb}_{1.7}\text{Te}_3$ ) thermoelectric element whose cross-sectional area and length are  $2.0 \text{ mm} \times 1.0 \text{ mm}$  and  $7.7 \text{ mm}$ , respectively, was used in this study, which were provided by Toshima Manufacturing Co., Ltd. A control electrode was attached on the left side of the thermoelectric element. We call the device loaded with the MA, fullerene, and control electrodes as the MA device, fullerene device, and control device, respectively as shown in Fig. 1a, c, d. The material properties of the  $\text{Bi}_{0.3}\text{Sb}_{1.7}\text{Te}_3$  are listed in Supplementary table S1.

Figure 1e presents comparison of a relative absorption spectra of the MA, fullerene (thickness: 300 nm), control electrodes, and a blackbody radiation spectrum calculated at 364 K. (Refer to Supplementary text S2.) IR measurements were conducted using a microscopic FITR (JASCO Corporation, FT/IR-6300, VIRT-3000). In the measurements, the reference spectra for all samples were recorded on a bare Cu electrode, which has a slight absorption in IR region owing to its intrinsic absorption. The relative absorption spectrum indicates the difference in absorption spectra between the sample and the reference. The MA has a strong absorption at  $5.3 \mu\text{m}$ , which is attributed to the magnetic resonance mode (Fig. S1) [22, 24, 25]. In contrast, the fullerene and control electrodes showed extremely low absorption. Figure 1(f) represents an enlarged relative absorption spectra of the fullerene and control electrodes. The control electrode showed a positive relative absorption, indicating that the control electrode has a higher absorption than the bare Cu electrode, originating

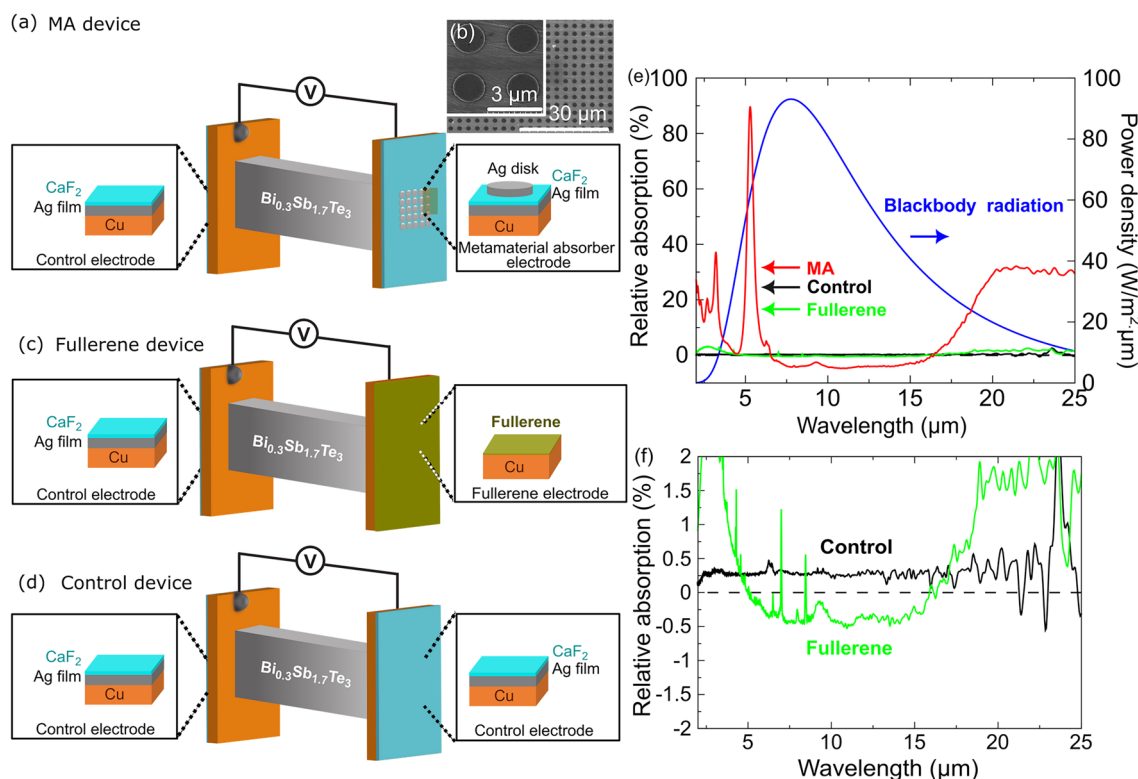


**Fig. 1** Schematics of the **a** MA, **c** fullerene, and **d** control thermoelectric devices. **b** SEM images of the MA. The inset is an enlarged image. The scale bars are 3–30  $\mu\text{m}$ , respectively. **e** Comparison of relative absorption spectra of the MA, fullerene, and control electrodes, and a blackbody radiation spectrum calculated at 364 K. The film thickness of the fullerene layer is 300 nm. **f** Enlarged absorption spectra of the fullerene and control electrodes

from an absorption of  $\text{CaF}_2$  layer with a thickness of 60 nm on a Ag layer of 150 nm in a wavelength range from 4 to 15  $\mu\text{m}$ . Interestingly, the relative absorption of the fullerene layer was lower than zero, meaning that the fullerene layer suppressed absorption of a bare Cu because a bulk Cu has a slight IR absorption as indicated in numerical calculation (Fig. S3a brown line) [26, 27]. Furthermore, numerical calculations of the relative absorption of the control and fullerene electrodes exhibited behavior similar to the experimental data specifically within the wavelength range of 2 – 18  $\mu\text{m}$ . This consistency suggests that the measured relative absorption of the control and fullerene electrodes is reliable, as shown in Fig. S3b. Due to the different absorptivity of each electrode, different thermoelectric properties are expected to arise in thermoelectric devices loaded with each electrode.

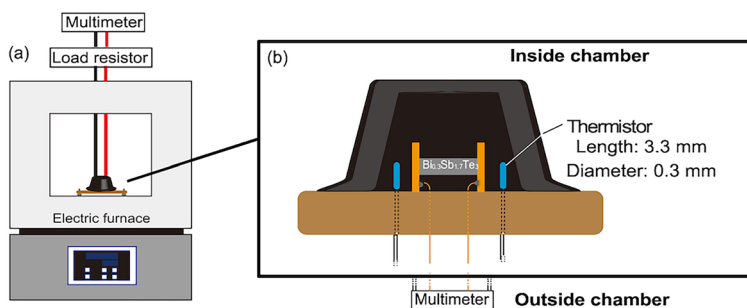
Figures 2 and S4 show the schematics and photographs of the experimental setup for measuring thermoelectric performance in an environment with uniform thermal radiation. To create an environment with uniform thermal radiation, we used an electric furnace (FUL210FA, Advantec) (Fig. 2a). For measuring thermoelectric performance, each device was fixed on a printed circuit substrate using a double Kapton tape as a spacer. Thermal conductivities of a printed circuit substrate and a Kapton tape are extremely low, indicating that these materials serve as a thermal and electrical insulator to isolate the thermoelectric device from a furnace chamber floor and other materials. Au wires with a diameter of 0.1 mm were connected to each electrode by Ag paste, and the Au wires are connected to Cu wires with a diameter of 0.1 mm to make an electrical contact between the thermoelectric device and a multimeter put outside of the furnace. A load resistor of 220 m $\Omega$  was included in the circuit to maximize the thermoelectric output power.

To prevent convection current created by air movement in the furnace chamber, the whole thermoelectric device was capped with a carbon pod whose diameter and height are 2.75 cm and 1.40 cm, respectively. Well-calibrated two thermistors were put 2 mm away from each electrode surface to monitor the temperature in the vicinity of each electrode. We defined the temperatures monitored by these thermistors as an environmental temperature. The printed circuit substrate holding the thermoelectric device and carbon pod was placed in the center of the furnace chamber and the device was heated after closing the chamber door. Details for experiments were described in Supplementary Information S3.

### 3 Results and Discussions

Figure 3a shows the dependence of output voltages generated by the MA, fullerene, and control devices on the measured environmental temperature. The plots in the output voltage and environmental temperature in Fig. 3a were obtained from the time dependence of the measured output voltage and temperatures on the environmental temperature as shown in Fig. S2. The output voltage of each device was taken as the value measured when the temperature and output voltage became stable. The MA device showed an output voltage of  $19.0 \pm 0.0 \mu\text{V}$  at an environmental temperature of 364 K, while the control device showed an output voltage of  $0.9 \pm 1.4 \mu\text{V}$ , which is around 20 times smaller than that generated by the MA device. Furthermore, the MA showed a positive output voltage at all environmental temperatures ranging from 323 to 434 K. The wiring connecting the MA device was configured to register a positive output voltage when the temperature of the MA electrode became higher, indicating that the temperature of the MA electrode is higher than that of the control electrode owing to thermal radiation absorption of the MA. The reason for the linear correlation between the measured output voltage and environmental temperature is the thermal radiation absorption of the MA increases with the environmental temperature within this range, leading to an increase in output voltage. Of course, this wiring setup was consistently employed in all experiments. We paid close attention to the device arrangement and length of the wiring in our experiment to ensure that no other factors influenced the thermoelectric properties (Supplementary Information S3).

**Fig. 2** Experimental setup for measuring thermoelectric performance. Schematics of (a) an electric furnace and (b) a thermoelectric device capped with a carbon pod



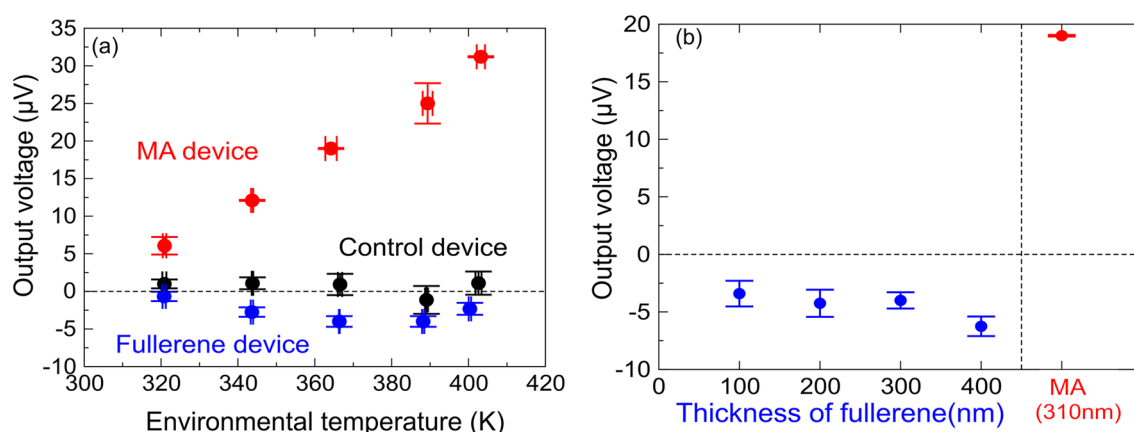


**Fig. 3** **a** Dependence of output voltages generated by the MA (red plots), fullerene (blue plots), and control (black plots) devices on the environmental temperature. Each device consists of a single *p*-type thermoelectric leg. **b** Dependence of the output voltages on the fullerene thicknesses varied from 100 to 400 nm measured at an environmental temperature of 364 K. The output voltage of the MA device is shown as a comparison

This output generation can be explained by the unbalanced absorptivity between the MA and control electrodes. Because the MA absorbs thermal radiation emitted from the surrounding medium and creates plasmonic local heat as plasmon loss, a thermal gradient is created across a thermoelectric element. This occurs through the conductive propagation of plasmonic local heat through the Cu electrode, resulting in thermoelectric output voltage generation. In other words, the plasmonic local heat generated by the MA is transferred to the opposite end and then to the load resistor located outside of the furnace chamber, where the thermal energy is released into the surrounding environment [12–14]. This indicates that the metamaterial thermoelectric conversion facilitates thermal exchange between the inside and outside of the furnace chamber, ensuring the device never reaches thermal equilibrium (Supplementary text S4). On the other hand, the control device did not show significant output voltages at every environmental temperature as the control electrodes at both ends have almost no IR absorptivity, leading to no thermal gradient across the thermoelectric element.

In contrast, the fullerene device showed a negative output voltage of  $-4.0 \pm 0.6 \mu\text{V}$  at an environmental temperature of 364 K, indicating the temperature of the fullerene electrode is lower than that of the control electrode, which is attributed to the slight difference in absorptivity between the fullerene and control electrodes as shown in Fig. 1c. Additionally, this tendency was observed in every environmental temperature. Generally, all materials exhibit thermal radiation absorption depending on their material properties. Thermal radiation absorption generally induces molecular vibrational energy, causing the material to generate heat. Therefore, the slight difference in absorptivity between the two electrodes leads to different amount of thermal radiation absorbed by the fullerene and control electrodes, which arises due to the inherent infrared absorption characteristics of these electrodes.

To investigate the possibility of observing negative output voltage, we varied the thickness of the fullerene layers from 100 to 400 nm. Figure S5 presents the measured relative absorption spectra of fullerene electrodes with various film thicknesses. Figure 3b represents the dependence of output voltages on the fullerene thicknesses with a comparison of the MA thickness (310 nm) at an environmental temperature of 364 K. The output voltage was linearly decreased as the film thicknesses were varied from 100 to 400 nm, meaning that the fullerene device consistently showed negative output voltages regardless of its film thickness. These results indicate an important insight that even a slight difference in absorptivity between electrodes at both ends would change the direction of thermal flow across a thermoelectric element in an environment with uniform thermal radiation.

As proof of this concept, we conducted a thermoelectric simulation of single-leg thermoelectric devices loaded with the MA or fullerene electrodes in an environment with uniform thermal radiation. Prior to thermoelectric simulation, we numerically evaluated the heat power density of the MA, fullerene,  $\text{Bi}_2\text{Te}_3$ , and bare Cu electrodes, respectively, using finite element method, COMSOL Multiphysics with Radio Frequency module. In the simulation,  $\text{Bi}_2\text{Te}_3$  was used as the thermoelectric material in place of  $\text{Bi}_{0.3}\text{Sb}_{1.7}\text{Te}_3$ . The material properties of the  $\text{Bi}_2\text{Te}_3$  used for thermoelectric simulations are listed in Table S1. The heat power density can be calculated using Eq. (1),



$$Q = \frac{1}{2} \text{Im}(\varepsilon(\omega)) \varepsilon_0 |\mathbf{E}(\mathbf{r})|^2, \quad (1)$$

where  $\varepsilon_0$  is the vacuum permittivity,  $\varepsilon(\omega)$  is the relative permittivity of the material, and  $|\mathbf{E}(\mathbf{r})|^2$  is the intensity of the electric field, respectively. [28] Figures S3 and S5 present calculated absorption spectra of the MA, fullerene (thickness of 300 nm), control, and a bare Cu electrodes, respectively. A blackbody radiation spectrum calculated at 364 K was shown as a comparison in Fig. 2a, b. As mentioned above, the bare Cu electrode has slight absorption in wavelength range from 2 to 15  $\mu\text{m}$ , where the blackbody radiation spectrum at 364 K peaks (Fig. S3a). The control electrode consisting of Ag and  $\text{CaF}_2$  thin layers has slightly larger absorption than that of the Cu electrode, which coincides with the measured results. This absorption is anticipated to arise from the  $\text{CaF}_2$  layer. In contrast, the fullerene layer serves to suppress absorption of the Cu electrode, leading to lower relative absorption in the wavelength range from 5 to 18  $\mu\text{m}$  as shown in Fig. 1f.

The calculated absorbed power densities of the MA, fullerene, control, a bare Cu, and  $\text{Bi}_2\text{Te}_3$  were  $4.1 \times 10^8$ , 0.02,  $4.1 \times 10^5$ ,  $4.2 \times 10^4$ ,  $1.8 \times 10^6 \text{ W m}^{-3}$  respectively. In thermoelectric simulation, the calculated absorbed power density is applied to each material unit every second to simulate the thermal distribution across the thermoelectric element by considering local heat generation at each material. These settings are required because all materials consisting of the device generate local heat depending on its absorption properties. The details are described in Supplementary Information S5.

Table 1 presents the measured and simulated output voltages of the MA, fullerene, and control devices with a single *p*-type  $\text{Bi}_{0.3}\text{Sb}_{1.7}\text{Te}_3$  thermoelectric legs. The simulated output voltage of each device showed good consistency with the measured values, indicating that calculated absorbed power density of each material is reasonable. Moreover, we verified that the simulated negative output voltage generation in the fullerene device was consistent with the measured results.

These results indicate that sophisticated control of the absorptivity at both ends of a thermoelectric device enables us to control the thermal flow direction, leading to thermoelectric generation in a  $\pi$ -shaped thermoelectric device consisting only of *p*-type thermoelectric elements in an environment with uniform thermal radiation. To verify this inference, we examined the performance of a  $\pi$ -shaped thermoelectric device comprising *p*-type legs.

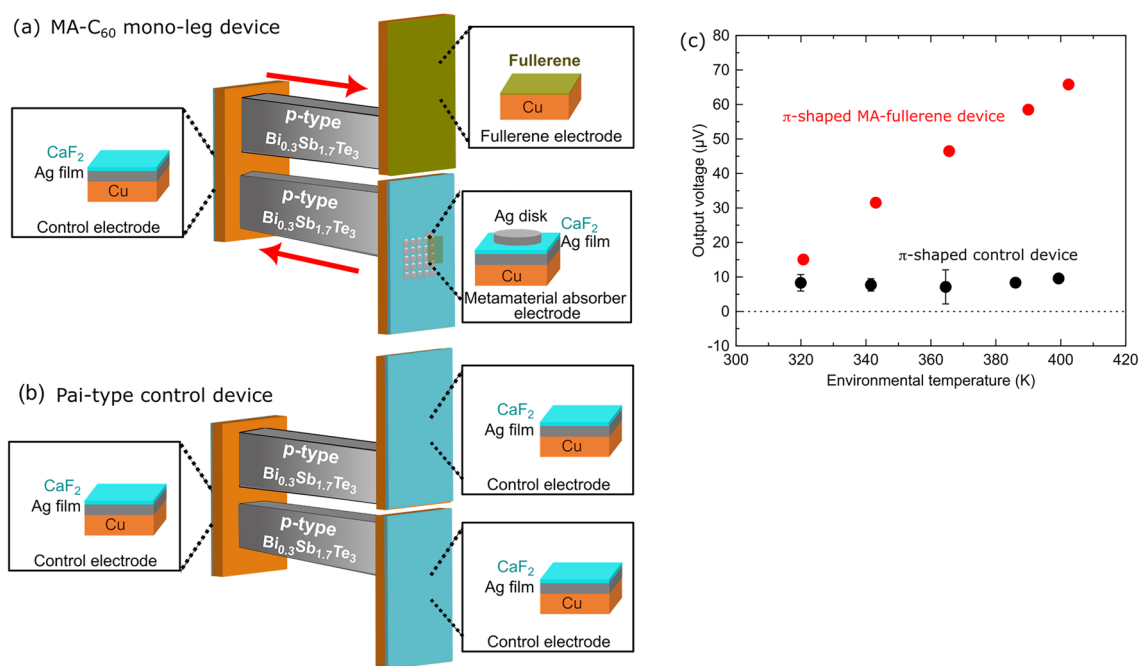
Figure 4a presents a schematic of the  $\pi$ -shaped MA-fullerene device consisting only of *p*-type  $\text{Bi}_{0.3}\text{Sb}_{1.7}\text{Te}_3$  thermoelectric elements. The MA and fullerene electrodes were attached on the right side of the *p*-type thermoelectric legs, and control electrodes, on the left side. It should be noted that the  $\pi$ -shaped MA-fullerene device consists only of *p*-type thermoelectric legs. In addition, a conventional  $\pi$ -shaped thermoelectric device with only *p*- or *n*-type thermoelectric legs would be incapable of generating electricity, as the carrier migration directions within two legs are identical, leading to carrier dissipation. Based on the absorptivity difference among the MA, fullerene, and control electrodes, we expect thermal gradients from the MA to control electrodes and from the control to the fullerene electrodes will be created as indicated by red arrows in Fig. 4a, by putting the device in an environment with uniform thermal radiation. Figure 4b represents a schematic of the  $\pi$ -shaped control thermoelectric device consisting only of *p*-type  $\text{Bi}_{0.3}\text{Sb}_{1.7}\text{Te}_3$  elements. The three control electrodes were attached on each side. In this device, no thermal flow is expected as the absorptivity of the control electrodes is ideally the same.

Figure 4c shows the dependence of the output voltage generated by the  $\pi$ -shaped MA-fullerene device on the environmental temperatures. The MA-fullerene device showed an output voltage of  $46.5 \pm 0.5 \mu\text{V}$  ( $n=4$ ) at an environmental temperature of 364 K. In contrast, the  $\pi$ -shaped control thermoelectric device exhibited output voltages of  $7.1 \pm 4.9 \mu\text{V}$  ( $n=4$ ) at the same environmental temperature. We considered that the slight output voltage generation observed for the  $\pi$ -shaped control thermoelectric device is due to the asymmetrical structure of the device. As the  $\pi$ -shaped device structure is asymmetrical on both sides, and all materials absorb thermal radiation, it is natural for the  $\pi$ -shaped device to generate a slight output voltage.

Furthermore, when the environmental temperature was varied, the output voltage of the  $\pi$ -shaped MA-fullerene thermoelectric device increased proportionally with the environmental temperature, whereas the  $\pi$ -shaped control

**Table 1** Comparison of measured and simulated output voltages of the MA, fullerene, and the control thermoelectric devices with a *p*-type  $\text{Bi}_{0.3}\text{Sb}_{1.7}\text{Te}_3$  thermoelectric leg

Device	Left electrode	Right electrode	Measured output voltage ( $\mu\text{V}$ )	Simulated output voltage ( $\mu\text{V}$ )
MA	Control electrode	MA electrode	$19 \pm 0.0$	14.4
Fullerene	Control electrode	Fullerene electrode	$-4.0 \pm 0.6$	-1.4
Control	Control electrode	Control electrode	$0.9 \pm 1.4$	–



**Fig. 4** Schematics of **a** the  $\pi$ -shaped MA-fullerene thermoelectric device and **b** the  $\pi$ -shaped control device. The red arrows on the  $\pi$ -shaped MA-fullerene device represent the directions of thermal flow across thermoelectric elements. **c** Comparison of thermoelectric output voltages of the  $\pi$ -shaped MA-fullerene device (red plots) and the  $\pi$ -typed control device (black plots) as a function of environmental temperature

thermoelectric device showed an output voltage of approximately 10  $\mu$ V, regardless of the environmental temperature. These facts imply that, on the  $\pi$ -shaped MA-fullerene thermoelectric device, a thermal flow from the MA to fullerene electrodes via the control electrode occurred as we expected. Of course, it should be noted that the output voltage generated by these devices includes components derived from the geometry of the  $\pi$ -shaped device. In fact, the output voltage for the  $\pi$ -shaped MA-fullerene thermoelectric device was larger than the combined output voltages of the MA and fullerene devices at an environment of 364 K, 24  $\mu$ V. However, the output voltage observed for the  $\pi$ -shaped MA-fullerene thermoelectric device was significantly higher comparing to that for the  $\pi$ -shaped control thermoelectric device. We concluded that, by tuning the absorptivity at both ends of a thermoelectric device, we could control thermal flow directions arbitrarily, leading to thermoelectric power generation even on the  $\pi$ -shaped MA-fullerene device comprising mono-legs in an environment with uniform thermal radiation.

It should be noted that the  $\pi$ -shaped MA-fullerene device only with *p*-type legs is valid only in an environment with uniform thermal radiation as a thermal gradient created by the surrounding environment would induce an identical direction of thermal flows on single-legs, leading to carrier dissipation. However, the ability to achieve power generation in an environment with uniform thermal radiation using a device with only a single type of thermoelectric element represents a paradigm shift in both the fabrication process of thermoelectric devices and the environments in which they can generate power.

## 4 Conclusion

We prepared the MA, fullerene, and control electrodes whose absorptivity is different in the IR region and examined the thermoelectric performance of the device loaded with these electrodes in an environment with uniform thermal radiation. We observed that the direction of thermal flows across the thermoelectric element depends on the absorptivity difference between the electrodes at two ends of a thermoelectric leg. The MA thermoelectric device induced a positive output voltage of  $19.0 \pm 0.0 \mu$ V, at an environment with uniform thermal radiation at 364 K, owing to strong absorption characterized by the MA, whereas the fullerene device exhibited a negative output voltage of  $-4.0 \pm 0.6 \mu$ V at 364 K, which is attributed to the slight difference in absorptivity between the fullerene and control electrodes. This result indicates that even a slight difference in absorptivity between the electrodes of a thermoelectric device can influence the

direction of thermal flow across thermoelectric elements in an environment with uniform thermal radiation. Given that this issue has not been thoroughly discussed, this insight is expected to contribute to the development of guidelines for conventional thermoelectric devices. This fact suggests that we need to be careful of certain aspects when using thermoelectric conversion devices in sensors [29]. For example, using a thermoelectric device to monitor a slight temperature difference in a micro space, a slight absorptivity difference between electrodes affects thermoelectric performance due to unexpected voltage. Furthermore, asymmetrical electrode geometry at both ends also generates absorptivity difference between the ends, leading to unexpected thermoelectric performance.

Building upon this scheme for controlling the direction of thermal flows, we observed an output voltage generation even on the  $\pi$ -shaped MA-fullerene device, which consists only of *p*-type thermoelectric legs in an environment with uniform thermal radiation. Their thermoelectric performance will be further improved through geometric optimization of metamaterial absorber [30]. In practical application, the use of the  $\pi$ -shaped MA-fullerene thermoelectric device is constrained, as it efficiently generates power only in an environment with uniform thermal radiation. Nevertheless, these discoveries offer valuable insights as a device guideline for conventional thermoelectric devices, given the lack of prior discussions on controlling the thermal absorption of device electrodes, materials, and configurations. Our investigation has clarified that even a slight difference in absorptivity between the electrodes of thermoelectric devices affect the direction of thermal flow, resulting in output voltage generation.

**Acknowledgements** The authors thank TOSHIMA Manufacturing Co., Ltd. for providing the *p*-type  $\text{Bi}_{0.3}\text{Sb}_{1.7}\text{Te}_3$  and *n*-type  $\text{Bi}_2\text{Te}_3$  thermoelectric legs.

**Author contribution** W.K. conceived the idea of this study. S.S. and A.Y. performed the fabrication and measurements with support from W.K. and T.T. T.T. and Y.L. coordinated the numerical calculations. All authors wrote the manuscript and contributed to the analysis and interpretation of results. W.K. supervised and coordinated the work.

**Funding** SEKISUI CHEMICAL CO. LTD, JSPS KAKENHI Grant Number JP24H02232, Kyoso Grant, National Science and Technology Council, NSTC-113-2112-M-001-014, Academia Sinica of Taiwan, AS-TP-113-M02.

**Data availability** Data is provided within the manuscript or supplementary information files.

## Declarations

**Competing Interests** The authors declare no competing interests.

**Open Access** This article is licensed under a Creative Commons Attribution-NonCommercial-NoDerivatives 4.0 International License, which permits any non-commercial use, sharing, distribution and reproduction in any medium or format, as long as you give appropriate credit to the original author(s) and the source, provide a link to the Creative Commons licence, and indicate if you modified the licensed material. You do not have permission under this licence to share adapted material derived from this article or parts of it. The images or other third party material in this article are included in the article's Creative Commons licence, unless indicated otherwise in a credit line to the material. If material is not included in the article's Creative Commons licence and your intended use is not permitted by statutory regulation or exceeds the permitted use, you will need to obtain permission directly from the copyright holder. To view a copy of this licence, visit <http://creativecommons.org/licenses/by-nc-nd/4.0/>.

## References

1. Zhang X, Zhao L-D. Thermoelectric materials: energy conversion between heat and electricity. *J Materiomics*. 2015;1:92–105.
2. Wang H, Yu C. Organic thermoelectrics: materials preparation, performance optimization, and device integration. *Joule*. 2019;3:53–80.
3. Hasan MN, Wahid H, Nayan NM, Ali MS. Inorganic thermoelectric materials A review. *Int J Energy Res*. 2020;44:6170–222.
4. Fitriani R, et al. A review on nanostructures of high-temperature thermoelectric materials for waste heat recovery. *Renew Sust Energ Rev*. 2016;64:635–59.
5. Shi X-L, Zou J, Chen Z-G. Advanced thermoelectric design: from materials and structures to devices. *Chem Rev*. 2020;120:7399–515. <https://doi.org/10.1021/acs.chemrev.0c00026>.
6. Zhang Y, Park S-J. Flexible organic thermoelectric materials and devices for wearable green energy harvesting. *Polymers*. 2019;11:909–27. <https://doi.org/10.3390/polym11050909>.
7. Tohidi F, Ghazanfari Holagh S, Chitsaz A. Thermoelectric Generators: A comprehensive review of characteristics and applications. *Appl Therm Eng*. 2022;201:117793.
8. Jaziri N, et al. A comprehensive review of Thermoelectric Generators: Technologies and common applications. *Energy Rep*. 2020;6:264–87.
9. Assaworarith S, Omair Z, Fan S. Nighttime electric power generation at a density of 50 mW/m<sup>2</sup> via radiative cooling of a photovoltaic cell. *Appl Phys Lett*. 2022. <https://doi.org/10.1063/5.0085205>.



10. Ishii S, Bourghès C, Tanjaya NK, Mori T. Transparent thermoelectric device for simultaneously harvesting radiative cooling and solar heating. *Mater Today*. 2024;75:20–6.
11. He R, Schierning G, Nielsch K. Thermoelectric devices: a review of devices, architectures, and contact optimization. *Adv Mater Technol*. 2018;3:1700256. <https://doi.org/10.1002/admt.201700256>.
12. Katsumata S, Tanaka T, Kubo W. Metamaterial perfect absorber simulations for intensifying the thermal gradient across a thermoelectric device. *Opt Express*. 2021;29:16396–405. <https://doi.org/10.1364/OE.418814>.
13. Asakura, T. *et al.* Metamaterial Thermoelectric Conversion. [arXiv:2204.13235](https://arxiv.org/abs/2204.13235) (2022). <<https://ui.adsabs.harvard.edu/abs/2022arXiv220413235A>>.
14. Nakayama R, Saito S, Tanaka T, Kubo W. Metasurface absorber enhanced thermoelectric conversion. *Nanophotonics*. 2024;13:1361–8.
15. Brongersma ML, Halas NJ, Nordlander P. Plasmon-induced hot carrier science and technology. *Nat Nanotechnol*. 2015;10:25–34. <https://doi.org/10.1038/nnano.2014.311>.
16. Baffou G, Cichos F, Quidant R. Applications and challenges of thermoplasmonics. *Nat Mater*. 2020;19:946–58. <https://doi.org/10.1038/s41563-020-0740-6>.
17. Kajikawa K, Takahara J. *Thermal Plasmonics and Metamaterials for a Low-Carbon Society*. Boca Raton: CRC Press; 2024.
18. Usman Javed M, et al. Tailoring the plasmonic properties of complex transition metal nitrides: A theoretical and experimental approach. *Appl Surf Sci*. 2023;641:158486.
19. Ciraulo B, García-Guirado J, de Miguel I, Ortega Arroyo J, Quidant R. Long-range optofluidic control with plasmon heating. *Nat Commun*. 2021;12:2001. <https://doi.org/10.1038/s41467-021-22280-3>.
20. Ishii S, Sugavaneshwar RP, Nagao T. Titanium Nitride Nanoparticles as Plasmonic Solar Heat Transducers. *J Phys Chem C*. 2016;120:2343–8. <https://doi.org/10.1021/acs.jpcc.5b09604>.
21. Kawamura N, Tanaka T, Kubo W. Nonradiative Cooling. *ACS Photonics*. 2024;11:1221–7. <https://doi.org/10.1021/acsp Photonics.3c01757>.
22. Landy NI, Sajuyigbe S, Mock JJ, Smith DR, Padilla WJ. Perfect Metamaterial Absorber. *Phys Rev Lett*. 2008;100:207402.
23. Tittl A, et al. Plasmonic absorbers: a switchable mid-infrared plasmonic perfect absorber with multispectral thermal imaging capability. *Adv Mater*. 2015;27:4597–603. <https://doi.org/10.1002/adma.201502023>.
24. Liu X, Xia F, Wang M, Liang J, Yun M. Working mechanism and progress of electromagnetic metamaterial perfect absorber. *Photonics*. 2023;10:205.
25. Cao T, Wei C-W, Simpson RE, Zhang L, Cryan MJ. Broadband polarization-independent perfect absorber using a phase-change metamaterial at visible frequencies. *Sci Rep*. 2014;4:3955. <https://doi.org/10.1038/srep03955>.
26. Biondi MA, Guobadia AI. Infrared absorption of aluminum, copper, lead, and nickel at 4.2 K. *Phys Rev*. 1968;166:667–73.
27. Biondi MA. Optical and Infrared Absorption of Copper at 4.2 K. *Phys Rev*. 1954;96:534–5.
28. Baffou G, Quidant R. Thermo-plasmonics: using metallic nanostructures as nano-sources of heat. *Laser Photonics Rev*. 2013;7:171–87.
29. Hirobe S, Wredh S, Yang JKW, Kubo W. Metamaterial thermopile beyond optical diffraction limit. *Appl Therm Eng*. 2024;256:124080.
30. Murakami K, Kubo W. Optimizing broadband metamaterial absorber using deep reinforcement learning. *Appl Phys Express*. 2023;16:082007.

**Publisher's Note** Springer Nature remains neutral with regard to jurisdictional claims in published maps and institutional affiliations.